A comparison of photolytic, photochemical and photocatalytic processes for disinfection of recirculation aquaculture systems (RAS) streams

Moreno-Andrés Javier, Rueda-Márquez Juan José, Homola Tomáš, Vielma Jouni, Moríñigo Miguel Ángel, Mikola Anna, Sillanpää Mika, Acevedo-Merino Asunción, Nebot Enrique, Levchuk Irina

DOI: 10.1016/j.watres.2020.115928

A comparison of photolytic, photochemical and photocatalytic processes for disinfection of recirculation aquaculture systems (RAS) streams

Javier Moreno-Andrés[1,8*], Juan José Rueda-Márquez[2], Tomáš Homola[3], Jouni Vielma[4], Miguel Ángel Moríñigo[5], Anna Mikola[6], Mika Sillanpää[7], Asunción Acevedo-Merino[1], Enrique Nebot[1], Irina Levchuk[6]

[1] Department of Environmental Technologies, Faculty of Marine and Environmental Sciences. INMAR-Marine Research Institute, CEIMAR- International Campus of Excellence of the Sea. University of Cadiz. Spain.

[2] Department of Separation Science, School of Engineering Science, Lappeenranta-Lahti University of Technology LUT, Sammonkatu 12, 50130 Mikkeli, Finland.

[3]R&D Center for Low-Cost Plasma and Nanotechnology Surface Modifications (CEPLANT), Department of Physical Electronics, Faculty of Science, Masaryk University, Kotlářská 267/2, 611 37 Brno, Czech Republic

[4]Natural Resources Institute Finland, Survontie 9A, 40500 Jyväskylä, Finland

[5]Department of Microbiology, Faculty of Sciences. University of Málaga.

[6]Water and Wastewater Engineering Research Group, School of Engineering, Aalto University, PO Box 15200, FI-00076 Aalto, Finland

[7]Department of Civil and Environmental Engineering, Florida International University, Miami, Fl, USA

[8] Grupo de Procesos de Oxidación Avanzada, Departamento de Ingeniería Textil y Papelera, Universitat Politècnica de València, Campus de Alcoy, Alcoy, Spain

[*]Corresponding Author. Javier Moreno-Andrés. E-mail address: javier.moreno@uca.es

Abstract:

The development of technologically advanced recirculation aquaculture systems (RAS) implies the reuse of water in a high recirculation rate (>90%). One of the most important phases for water management in RAS involves water disinfection in order to avoid proliferation of potential pathogens and related fish diseases. Accordingly, different approaches have been assessed in this study by performing a comparison of photolytic (UV-LEDs) at different wavelengths (λ= 262, 268 and 262+268 nm), photochemical (UV-LEDs/H_2O_2, UV-LEDs/HSO_5^- and UV-LEDs/$S_2O_8^{2-}$) and

photocatalytic (TiO_2/SiO_2/UV-LEDs and ZnO/SiO_2/UV-LEDs) processes for the disinfection of water in RAS streams. Different laboratory tests were performed in batch scale with real RAS stream water and naturally occurring bacteria (*Aeromonas hydrophyla* and *Citrobacter gillenii*) as target microorganisms. Regarding photolytic processes, higher inactivation rates were obtained by combining $\lambda_{262+268}$ in front of single wavelengths. Photochemical processes showed higher efficiencies by comparison with a single UV-C process, especially at 10 $mg \cdot L^{-1}$ of initial oxidant dose. The inactivation kinetic rate constant was improved in the range of 15-38%, with major efficiency for $UV/H_2O_2 \sim UV/HSO_5^- > UV/S_2O_8^{2-}$. According to photocatalytic tests, higher efficiencies were obtained by improving the inactivation kinetic rate constant up to 55% in comparison with a single UV-C process. Preliminary cost estimation was conducted for all tested disinfection methods. Those results suggest the potential application of UV-LEDs as promoter of different photochemical and photocatalytic processes, which are able to enhance disinfection in particular cases, such as the aquaculture industry.

Key Words:

Advanced Oxidation processes, UVC-LEDs, recirculation aquaculture systems (RAS), natural occurring bacteria, UV inactivation, persulfate.

1. Introduction

Nowadays aquaculture industry is one of the most rapidly developing food sectors in the world (Badiola et al., 2012; Diana et al., 2013; Klinger and Naylor, 2012). Continuous growth of aquaculture production (in terms of freshwater, marine water and brackish water) move towards intensive cultivation systems (Badiola et al., 2012; Diana et al., 2013; Piedrahita, 2003). It promotes, among other options, the development of technologically advanced recirculation aquaculture systems (RAS) (Badiola et al., 2012; Klinger and Naylor, 2012; Martins et al., 2010). RAS offers several advantages, such as a decrease in water consumption, nutrients recycling and improved waste management, and also better biological control (Lund et al., 2013; Martins et al., 2010).

One of the main characteristics and advantage of the RAS, is the high capacity for water reuse, where the recirculation rate is > 90% (Martins et al., 2010; Vadstein et al., 2018). However, intensive regimes of fish feeding are leading to significant concentrations of organic matter and nutrients in RAS (Blancheton et al., 2013; Piedrahita, 2003). Intensive cultivation systems favor the growth of undesirable bacteria, which leads to potential proliferation of opportunistic (and mainly pathogenic) bacteria. This, in turn, may cause a poor performance of the system due to detrimental fish-microbe interactions (Attramadal et al., 2012b; Blancheton et al., 2013; Vadstein et al., 2018). Accordingly, appropriate microbial management strategies are needed.

The most important phases for water management in RAS usually involve detoxification of ammonia in a biofilter and water disinfection. For the latter, major disinfection treatment methods implemented are UV-C radiation, ozonation or hydrogen peroxide (Arvin and Pedersen, 2015; Summerfelt, 2003). Chemical treatments have high efficacy of disinfection, but they must be applied in a range of concentrations that do not damage the organisms reared or the nitrifying bacteria in the biofilters, and not

always those ranges are sufficient to reach disinfection (Arvin and Pedersen, 2015; Attramadal et al., 2012a; Pedersen and Pedersen, 2012).

The UV radiation is defined as a physical treatment, able to inactivate a wide range of bacteria. The germicidal range in the UV-C region (λ < 280 nm) is mostly applied in water treatment systems by low and medium pressure mercury lamps as a UV-C source. The efficacy of these UV-C sources is well known, and the UV doses needed to inactivate several pathogens (including bacteria, viruses, etc.) are well established (Malayeri et al., 2016). However, the potential toxicity of mercury from the lamps, their high cost, low efficiency and relatively short lifetime appears as the main concerns of this traditional source of UV-C (Song et al., 2016). A potential alternative is the use of emerging ultraviolet light-emitting diode (UV-LED) (Chen et al., 2017; Song et al., 2016). The main advantages of UV-LEDs are environmental friendliness (absence of mercury), compactness, robustness, potentially lower energy consumption and significantly longer lifetime. Although still low wall plug efficiency values and relatively high costs are main limitations of UV-C -LEDs (Matafonova and Batoev, 2018), several studies predict that these drawbacks will overcome in the next few years (Nyangaresi et al., 2018; Song et al., 2016). Recently, some studies assess the efficiency of UV-LEDs for water disinfection, nonetheless, some discrepancies were observed according to the dose response data and inactivation kinetics, so the application of UV-LEDs for water disinfection deserves deeper research (Chen et al., 2017; Song et al., 2016; Umar et al., 2019).

It is well known that the use of UV radiation can promote the generation of highly oxidizing radicals (•OH, $SO_4^{\bullet-}$) via photocatalytic (TiO_2, ZnO, etc.) or photochemical (H_2O_2, $S_2O_8^-$, HSO_5^-, etc.) pathway in the so-called Advanced Oxidation Processes (AOPs). AOPs are known to be efficient for water disinfection (Ganguly et al., 2018;

Levchuk et al., 2018; Rizzo et al., 2019; Rodríguez-Chueca et al., 2019; Xiao et al., 2019). With the appearance of UV-LEDs as emerging source for UV radiation, the research on AOPs using LEDs have also been intensified. For instance, the formation of •OH has been demonstrated in both photochemical and photocatalytic systems (Dominguez et al., 2015; Takeda et al., 2017). However, most of the studies have been performed with purified lab grade water and are primarily focused on the degradation of pollutants (Matafonova and Batoev, 2018), with only a few centered for disinfection purposes (Jo and Tayade, 2014; Levchuk et al., 2018; Martín-Sómer et al., 2017; Rodríguez-Chueca et al., 2017), which are majorly focused on the UV-A region. Accordingly, more research with real water matrices is required, since recent studies highlight the critical importance of choosing appropriately a realistic water matrix for the assessment of different oxidation processes (Lado Ribeiro et al., 2019; Matafonova and Batoev, 2018; Ribeiro et al., 2019).

In this scenario, the main goal of this study is to compare the disinfection efficacy of several UV-LED driven processes with different mode of action: photolytic treatment at different wavelength range (λ= 262, 268 and 262+268 nm), photochemical processes by the use of H_2O_2 and two different persulfate sources (HSO_5^-, $S_2O_8^{2-}$), and photocatalytic processes with TiO_2/SiO_2 and ZnO/SiO_2 photocatalytic thin films. These processes were tested with real RAS stream water and with naturally occurring microorganisms in the matrix. Finally, some considerations about the cost of tested treatment methods are presented.

2. Material and Methods

2.1 Water sampling and characterization

Real RAS stream water was used for experimentation. The experiment RAS platform is located at the Natural Resources Institute Finland (Luke), Laukaa fish farm. RAS system layout (fish tank, solids removal units, and moving and fixed bed bioreactors) are described in detail by Pulkkinen et al., (2018). Briefly, the RAS unit providing water for the trials, consists of a 500 L fish tank, a swirl separator, a drum filter with 60 μm filter panels (Hydrotech HDF501, Veolia, Paris, France), a 150 L moving bed biofilter (each filled with 70 L of plastic carrier media, RK Bioelements), and a trickling filter for carbon dioxide removal. Water pH was adjusted to 7.2 in pump sump with diluted sodium hydroxide using automated system (Prominent, Heidelberg, Germany). Oxygen saturation was kept above 80% in the fish tanks. The water temperature was maintained at 15 °C by controlling the room temperature.

The RAS unit had a total water volume of 890 liters, with a water flow of 720 liters per hour (the circulating water flow rate was set to 0.2 $L \cdot s^{-1}$) and water renewal of 500 liters per kg feed per day. During the water sampling campaign, tanks were stocked with 50 European whitefish (*Coregonus lavaretus*) and fed 140-190 $gr \cdot d^{-1}$.

Samples were taken directly after the fish tank, before water treatment units, and send to the laboratory in coolbox. Total ammonia nitrogen (TAN), nitrite and nitrate were monitored weekly by laboratory tests (Procedure 8038 Nessler, LCK341/342, LCK340), and alkalinity by a standard titration method (ISO 9963−1:1994, TitraLab AT1000, Hach, Loveland, USA). Some of these water quality parameters in the systems during the sampling procedures are detailed in Table S1. More detailed characterization with average water quality values is reported by Pulkkinen et al., (2018). Additionally,

several physical-chemical parameters of the water matrix were determined just before experimentation (Table 1). The pH and conductivity of test water were measured with inoLab 7110 pH-meter and conductivity meter Orion 101, respectively. The UV/Visible spectrophotometer (UV-1800 Shimadzu) was used for measuring transmittance of test water (λ = 262 nm; λ = 268 nm). Concentration of total organic carbon (TOC) was measured in non-purgeable organic carbon (NPOC) mode by means of TOC-V_{CSH} analyzer (Shimadzu, Japan).

Table 1. Characterization of RAS water matrix used in the experimentation.

2.2 Microbiological procedures

Naturally occurring bacteria from RAS stream were used as model microorganisms in the inactivation experiments. Thus, water samples were microbiologically analyzed. Isolation and purification of microorganisms were carried out following the quadrant streak technique over a series of commercial media: Slanetz & Bartley Agar (Panreac); Chromogenic Collinstant Agar (Scharlab) and Thiosulfate Citrate Bile Salts Sucrose Agar, TCBS (Pronadisa, Condalab). The plates were incubated at 35 ± 2 °C for 24 h. After the incubation period, colonies with good morphology were extracted and spread over the same media where initially isolated. Bacterial isolates were identified to species level by the amplification and sequentiation of a fragment of 16S rDNA. The partial 16S rDNA was amplified using universal primers, as previously explained (Levchuk et al., 2019). The results obtained are represented in Table 2.

Table 2. Bacterial identification in water samples from the RAS.

The concentration of bacteria in RAS was quantified in the range of 10^3 CFU·mL^{-1}. In order to reach high concentration of natural occurring bacteria and secure good statistics for kinetic modeling, yeast extract was added (5 µg·mL^{-1} added as once) as a substrate for wild bacteria. This will result in a bloom of fast-growing r-strategists, which is an

indicator of less specialists opportunistic pathogens that are detrimental to the fish (Vadstein et al., 2018). Besides, it also favors the percentage of cultivable bacteria (Salvesen et al., 1999). After 24 h of incubation, the dominance of bacterial species were *Aeromonas hydrophila* (ATCC 7966) and *Citrobacter gillenii* (SH1), which were used as model microorganisms for inactivation assays. Both species are gram-negative bacillus, γ- proteobacteria, which are usually found in the intestinal microbiota of fish, and also associated to fish diseases (Bruni et al., 2018; Rurangwa and Verdegem, 2015).

The evolution and survival of microorganisms after treatment was monitored with standard plate counts in Chromogenic Collinstant Agar (Scharlab) for *C. gillenii* and TCBS (Pronadisa, Condalab) for *A. hydrophila.* Plates were incubated at 35 ± 2 °C for 24 h. In order to ensure a measurable number of CFUs, tenfold dilutions from each sample were plated in triplicate.

2.3 Preparation and characterization of TiO_2/SiO_2 and ZnO/SiO_2 thin films

The preparation of ZnO/SiO_2 thin films was conducted as described below. The ink was prepared by mixing 24 mL of ZnO dispersion (20 wt% of nanoparticulate ZnO nanopowder of <100 nm particle size, 544906 Sigma Aldrich) in Dowanol® PM (1-methoxypropan-2-ol) with 8 mL of a recently-reported organosilica binder (Grégori et al., 2014) (20 wt% in anhydrous ethanol) and 24 mL of isobutanol. The ZnO/SiO_2 ratio was 75:25. Approx. 45 g of 1 mm glass balls were added to this in a 100 mL glass vial and this was placed on a mixer set to 90 rpm for 8 hours. The ZnO/SiO_2 films were deposited on polyethylene terephthalate (PET) using bar coater method using bars of wire diameter 30 µm and 50 µm. The materials and procedures employed for the printable suspension formulation have been reported in detail in our previous work (Homola et al., 2017, 2016).

For the preparation of TiO_2/SiO_2 coatings procedure reported in earlier studies was applied (Homola et al., 2016; Levchuk et al., 2019). Briefly, an experimental Fujifilm Dimatix 2831 inkjet printer was employed for the deposition of coatings on PET substrate. Mixture of dispersed TiO_2 (20 wt% of nanoparticulate titania Evonik P25 in Dowanol® PM (1-methoxypropan-2-ol), volume 6 mL) with organosilica binder (20 wt% in anhydrous ethanol; volume 2 mL) and isobutanol (8 mL) was used as an ink. Approx. 2 cm^3 of 1 mm glass balls were added to this in a 20 mL glass vial and this was located on an oscillating shaker (1000 rpm) overnight. The TiO_2/SiO_2 ratio was similar to ZnO/SiO_2 thin films and the thickness of the prepared films was about 300 nm.

To control the wettability of the photocatalytic surfaces, TiO_2/SiO_2 and ZnO/SiO_2 thin films were modified using RPS400 atmospheric-pressure ambient air plasma applied for 64 seconds (RPS400 for roll-to-roll, Roplass s.r.o., Czech Republic). The RPS400 was equipped with diffuse coplanar surface barrier discharge (DCSBD) plasma unit, which is capable of generating high-power-density surface plasma (100 W/cm^3) at a low temperature of 70 °C (Homola et al., 2016). The TiO_2/SiO_2 and ZnO/SiO_2 coatings were tested for disinfection after plasma treatment.

For evaluation of morphology of prepared TiO_2/SiO_2 and ZnO/SiO_2 thin films scanning electron microscope (SEM, MIRA3) was used. Chemical composition of prepared coatings was studied using X-ray photoelectron spectroscopy (XPS) using an Al Kα ESCALAB 250Xi apparatus (Thermo Fisher Scientific). Following parameters were applied for XPS measurements of all samples: 650 μm spots, a takeoff angle of 90°, 10^{-8} mbar vacuum, 20 °C. An electron flood-gun was used to compensate for charges on sample surfaces. The C 1s at 284.8 eV was applied to reference the spectra.

Crystalline properties of prepared TiO_2/SiO_2 and ZnO/SiO_2 thin films were measured by means of X-ray diffractometry (XRD). The SmartLab (Rigaku, Japan) diffractometer in

Bragg-Brentano geometry was used with 1.542Å Cu Kα. The Scherrer equation was applied to estimate crystallite sizes of prepared TiO_2/SiO_2 and ZnO/SiO_2 coatings. The OCA 15plus (NEURTEK Instruments) connected to the digital camera was used to measure the water contact angle on the surface of TiO_2/SiO_2 and ZnO/SiO_2.

2.4 Experimental set-up

Photolytic tests were conducted in batch mode at room temperature. UV-LED photoreactor was built with 11 LED components (Sensor Electronic Technology Inc. (SETi), Columbia). Two different sets of LEDs were used within the UV-C region, distinguishing according to the wavelength peak: 262 nm and 268 nm. The LEDs components were made of aluminium and gallium nitrides (AlInGaN) and were installed inside TO-39 semiconductor package with a flat quartz glass window (Rantalankila et al., 2016). Thus, the LED module consists of a concentric circle (diameter of 50 mm) with 3 LEDs on the inner and 8 LEDs on the outer circle. According to previous studies, the distance from the lamp to solution surface was set at 5 mm (Rantalankila et al., 2016). A 20 mL of test water (RAS stream) was poured in a borosilicate Petri dish (internal diameter of 51 mm) and gently stirred during the treatment. UV-C radiation was applied and varied via treatment time, i.e., samples were taken at regular exposure times from zero to five minutes.

The temperature, input voltage (24 V) and current (0.05A) of the LEDs were monitored with an external platinum resistance thermometer (Fluke 16) and a multimeter (Fluke 112). Ultraviolet irradiance was measured using a spectroradiometer with cosine receptor (Black-Stellarnet Comet C50-BW16) (Rantalankila et al., 2016). An average germicidal irradiance throughout the water volume was calculated in the range of 0.055-

0.069 $mW \cdot cm^{-2}$ (λ=262 nm) and 0.126-0.128 $mW \cdot cm^{-2}$ (λ=268 nm) respectively (Bolton and Linden, 2003).

Different tests were performed according to different processes. Firstly, photolytic tests were performed with single UV-C radiation at selected wavelengths of 262 and 268 nm. Both wavelengths were applied for solo and simultaneous exposure (λ_{262} - outer circle + λ_{268} - inner circle). Secondly, photochemical tests were performed with single UV-C wavelength (λ = 262 nm) and different chemicals: hydrogen peroxide, H_2O_2 (30%, Merck KGaA), sodium peroxydisulfate, PDS ($Na_2S_2O_8$, ≥98%, Sigma Aldrich) and potassium peroxymonosulfate, PMS ($KHSO_5 \cdot 0.5KHSO_4 \cdot 0.5K_2SO_4$, Oxone©, Sigma-Aldrich). Different oxidants were added in a single dosage and at different concentrations: 1, 5 and 10 $mg \cdot L^{-1}$. Concentrations of H_2O_2, PDS and PMS were determined spectrophotometrically at the beginning and at the end of each experiment according to the protocols proposed by Eisenberg, (1943); Liang et al., (2008) and Wacławek et al., (2015).

Finally, photocatalytic tests were performed with thin films prepared as explained in section 2.3. TiO_2 and ZnO were chosen as the most commonly used photocatalysts (Byrne et al., 2018). A TiO_2/SiO_2 and ZnO/SiO_2 thin films with geometrical surface area of 12.25 cm^2 were placed into Petri dish and photo-activated with UV-LEDs (λ = 262 nm). Prior UV-C exposure, the reactor with photocatalyst and test water was left stirring during 15 min in the dark. Volume of test water and distance from the surface of the water and the LEDs were 20 mL and 5 mm, respectively.

For all tested systems, a sample was kept in the dark and was taken as control tests for the different processes but without the intervention of UV-C light, i.e., same conditions with chemical concentrations and photocatalysts but in the dark. They were analyzed at regular intervals within the regular experimental procedures. In this case, the damage

caused by the chemical itself or possible adhesion onto the photocatalyst surface was quantified. The effect caused by the oxidants was negligible. Adsorption results are reported in Section 3.3.2.

2.5 Data analysis

Microbial inactivation was assessed through the definition of UV-dose response curves. A standard protocol for determining the UV-dose in LED reactors is still not defined (Song et al., 2016). Hence well-stablished protocol of Bolton and Linden, (2003) was followed. It contemplates operating parameters such as the water factor, petri factor, etc. It has been successfully applied in previous studies (Li et al., 2017; Oguma et al., 2016; Song et al., 2019). Thus, an approximation of UV-dose applied can be obtained.

The logarithmic reduction of the survival microorganisms (Log (N/N_0)) was obtained and represented according to the mean bacterial counts of each sampling time. According to the initial concentration of microorganisms (~10^6 CFU·mL^{-1}), the detection limit was defined as 5.51 – 6.30 decimal log reductions.

The disinfection profiles depicted a decrease in the bacteria survival with respect to the irradiance time and the applied UV dose. For batch operation mode, usually there is a first section in which the disinfection rate is higher followed by a second section with a lower disinfection rate (tailing) (Marugán et al., 2008; Romero-Martínez et al., 2014). These features accord with the Log-linear plus tail model commonly applied in UV disinfection processes with different types of organisms (Mattle and Kohn, 2012; Moreno-Andrés et al., 2019, 2017). It was calculated from experimental data obtained and according to Eq. (1). Parameters obtained as k_{max} (disinfection rate constant based on UV-dose, $cm^2 \cdot mJ^{-1}$) are useful for a better understanding of inactivation routes. The coefficient of determination (R^2), supported with the Root Mean Square Error (RMSE),

was used to assess the goodness of model fit. These values together with the specific model parameterization were obtained through GinaFiT tool (Geeraerd et al., 2005).

$$N = (N_0 - N_{res}) \cdot e^{-k_{max}\, UV\ Dose} + N_{res} \qquad \text{Eq. (1)}$$

3. Results and discussion

3.1 Photolytic treatment

Inactivation profiles from photolytic processes are represented in Figure 1. The good adjustment of the experimental points to the Log-linear + tail model (R^2>0.97, RMSE=0.259-0.418) shows a first log-linear decay period that follows a specific inactivation rate (k_1) which acquires importance until reaching the 5 Log Removal Value (LRV). This 5 LRV is in the range of 7.5-10.75 mJ·cm^{-2}, depending on the wavelength and the bacterial indicator. Accordingly, major inactivation occurs within the first decay phase, which means that 99.999% of inactivation follows the first inactivation rate, so k_{max} is the most significant kinetic parameter. It has been obtained for both organisms and for the three different wavelengths (Fig. 2).

Figure 1. Inactivation profiles obtained for photolytic processes and for two different naturally occurring bacteria in RAS streams. **A.** *A. hydrophila* and **B.** *C. gillenii*. Experimental points are fitted to Log-lineal + tail inactivation model (lines). The coefficient of variation of each experimental point does not exceed 15%.

According to the different organisms, similar kinetic rate constants have been obtained for the three different wavelengths (Fig. 2). It suggests similar UV sensitivity for both *A. hydrophila* and *C. gillenii*. UV wavelengths are in the range 262-268 nm, in which the nucleic acids have higher absorbance, and thus may be the main cause of inactivation (Hull and Linden, 2018; Rattanakul and Oguma, 2018). In this case, both bacteria are gram-negative and opportunists, with high sensitivity to UV treatments, since this type of bacteria are characterized by a fast growth under optimal conditions but low ability to compete and survive under stress conditions (Vadstein et al., 2018).

In this study, the 5 LRV for both bacteria has been reached in the range of 8.52-9.83 mJ·cm^{-2}. It agrees with values obtained for the same bacterial groups under traditional

mercury lamps (UV_{254nm}) (Malayeri et al., 2016). This also agrees with a previous study in which 4 $mJ \cdot cm^{-2}$ (λ_{265}) achieved approximately 2 LRV for other opportunistic bacteria, such as *Pseudomonas aeruginosa* (Rattanakul and Oguma, 2018). If it is compared with typical indicators, e.g. *E. coli*, which is also a gram-negative bacterium, reported values are 2-3.3 $mJ \cdot cm^{-2}$ per LRV (Song et al., 2019, 2016). Those inactivation values suggest a similar range of inactivation if it is compared with the opportunistic bacteria tested in this study (Fig. 2).

Figure 2. Maximum kinetic rate constant of inactivation obtained for photolytic treatment at different wavelengths. k_{max} is expressed in terms of UV-Dose, $cm^2 \cdot mJ^{-1}$. Error bars represent Standard Error.

Slightly higher inactivation rates have been obtained when combination of LEDs (λ=262 + 268 nm) was used as irradiation source. Thus, the UV dose required for 5 LRV decrease of *A. hydrophila* and *C. gillenii* was 8.12 and 7.27 $mJ \cdot cm^{-2}$, respectively. This means that about 16-25% lower UV dose is required when combination of LEDs (λ=262 + 268 nm) is applied in comparison with LEDs emitting only at 262 nm or 268 nm. Obtained results are in agreement with earlier studies. For instance, Song et al., (2019), found an additive effect on the inactivation of *E. coli* by combination of $\lambda_{265+285}$. Beck et al., (2017) studied a close wavelength combination ($\lambda_{260+280}$) and reach only slight enhancement in *E. coli* inactivation; otherwise they conclude that the combination of wavelengths results in a significant advantage in terms of energy efficiency. Those studies (Beck et al., 2017; Song et al., 2019) focused on the effect of two different wavelengths in different regions, i.e, UV-B and UV-C. In this study, the dual wavelengths that have been combined are within UV-C region. It has been demonstrated that the percent of DNA damage within these wavelengths is about 80-93% for gram-negative bacteria (Kim et al., 2017). Thus, the slight enhancement of

inactivation by simultaneous exposure of $\lambda_{262+268}$ could be due to the same type of DNA damages (Song et al., 2019).

3.2 Photochemical treatment

Different photochemical processes have been investigated in order to accelerate UV-C disinfection, i.e., UV/H_2O_2, UV/HSO_5^- and UV/$S_2O_8^{2-}$ with *C. gillenii* as the bacterial indicator. The action of UV radiation, especially in the UV-C region, produces the homolysis of persulfate anion and H_2O_2 (Eq. 2-4) (Vilhunen et al., 2011; Xiao et al., 2019). Accordingly, the tests have been performed under more favorable conditions, i.e., in order to promote the major efficiency and radical production (primarily •OH and $SO_4^{\bullet-}$), the lowest wavelength (λ_{262}) have been used as a source of light (Vilhunen et al., 2011).

$$H_2O_2 + h\upsilon \rightarrow 2\ {}^{\bullet}OH \qquad \text{Eq. (2)}$$

$$S_2O_8^{2-} + h\upsilon \rightarrow 2\ SO_4^{\bullet-} \qquad \text{Eq. (3)}$$

$$HSO_5^- + h\upsilon \rightarrow SO_4^{\bullet-} + {}^{\bullet}OH \qquad \text{Eq. (4)}$$

Figure 3. Inactivation profiles obtained for three different photochemical processes: **A.** UV/H_2O_2, **B.** UV/PDS, and **C.** UV/PMS. Bacterial indicator: *Citrobacter gillenii.* The coefficient of variation of each experimental point does not exceed 25%.

Inactivation profiles with experimental data obtained are represented in Figure 3. As can be seen, different initial concentrations (1, 5 and 10 mg·L^{-1}) have been tested for each specific process. Inactivation profiles fit well with Log-linear + tail model, and kinetic parameters obtained are shown in Table 3 (for time-based k_{max}, the reader is referred to Table S4). As with the photolytic processes, major inactivation occurs in a first step (Nres > 5 LRV). So, major inactivation follows a linear k_{max}. In most of the cases, the addition of oxidants at concentrations tested is enough to accelerate the disinfection, as kinetic rate constant is generally higher in presence of H_2O_2, HSO_5^- and $S_2O_8^{2-}$ by comparison with the simple photolytic process.

For UV/H_2O_2, the higher the concentration means the higher the effectiveness. The best enhancement has been obtained with 10 mg·L^{-1}, which is able to accelerate k_{max} up to 38.2% by comparison with UV-C sole. The same scenario was obtained for UV/$S_2O_8^{2-}$, in which the increase of k_{max} have been quantified up to ~20% with 10 mg·L^{-1} of PDS. In the UV/HSO_5^- system, the best improvement, i.e., ~25% (based on the increase on k_{max}) have been obtained with 5 and 10 mg·L^{-1} of PMS. The addition of chemicals at 1 mg·L^{-1} does not show improvements for any of the systems.

Table 3. Kinetic parameters obtained after the application of different photochemical systems at different concentrations of H_2O_2, PDS and PMS. It has been obtained through modeling of experimental points through the Log-lineal+tail model (R^2 > 0.94; RMSE: 0.33-0.51). Bacterial indicator: *Citrobacter gillenii*.

According to the different process at 10 mg·L^{-1} of starting concentration, detection limit was reached at 6.98 mJ·cm^{-2} (UV/H_2O_2), 16.2 mJ·cm^{-2} (UV/PDS) and 9.9 mJ·cm^{-2} (UV/PMS). Those results suggest that hydroxyl radical-based processes were more active than sulfate radical-based processes (Bianco et al., 2017; Sun et al., 2016). Those studies concluded that disinfection efficiency was higher in those processes that involve •OH radicals than those where primary SO_4•$^-$ radicals are promoted. In the case of UV/HSO_5^-, the detection limit was reached equally with 5 or 10 mg PMS·L^{-1}, suggesting the higher effectiveness of this process (Fig. 3). It agrees with related studies, where major efficiencies were detected for PMS compound in front of $S_2O_8^{2-}$ or H_2O_2 (Rodríguez-Chueca et al., 2019). The activation mechanism of HSO_5^- involve the generation of both •OH and SO_4•$^-$. Also, the PMS compound present low stability and could easily react with dissolved ions to form secondary oxidants (Moreno-Andrés et al., 2019; Wen et al., 2019) that might be involved in disinfection mechanisms.

Accordingly, results obtained agree with available literature, which generally indicates the feasibility of UV-LEDs for different photochemical processes. In parallel, the case

of disinfection studies performed with real water matrices are scarce. Recently, Rodríguez-Chueca et al., (2019) tested these processes in real wastewater matrices, and reach improvements up to 25% in comparison with UV-C, which is in accordance with our results. Slightly higher efficiency of *K. pneumoniae* inactivation with UV/$S_2O_8^{2-}$ and UV/H_2O_2 (by comparison with UV-C) in real wastewater matrix was reported by Serna-Galvis et al., (2020). Nonetheless, they detected that the UV-C light had a strong and fast disinfecting action, which was also observed in our study. Thus, the beneficial effect of photochemical processes might not be easily appreciable. Accordingly, the use of UV-resistant microorganisms is encouraged in order to clearly study the role of AOPs. Those studies accord with our results, since similar levels of enhancement have been obtained with similar range of concentrations. Hence, the use of UV-LEDs as radiation source is suggested, as they can be efficiently used for light-driven photochemical processes.

The use of oxidants in RAS must be carefully evaluated regarding the potential impact on biofilter performance, which ideally will be after disinfection phase (Arvin and Pedersen, 2015; Vadstein et al., 2018), as well as to maintain fish welfare. Some studies have been performed in order to study the decomposition rates of some oxidants, such H_2O_2 by determining that low concentrations of H_2O_2 (< 20 $mg \cdot L^{-1}$) can reach a complete decomposition within a few hours (Arvin and Pedersen, 2015; Pedersen et al., 2019). These concentration levels are in agreement with concentrations used in our study. In addition, consumption rates of the several oxidants used have been quantified after the application of UV-C light being 0.82-14.81% for H_2O_2, 1.21-17.02% for $S_2O_8^{2-}$, and 1.69-20.21% for HSO_5^-. So, the application of photochemical processes not only can achieve faster and most efficient disinfection at low concentrations of oxidants but also promote degradation of the oxidants by photolysis of the chemicals.

3.3 Photocatalytic treatments

3.3.1 Characterization of printed TiO_2/SiO_2 and ZnO/SiO_2 thin films

The surface properties of ZnO/SiO_2 and TiO_2/SiO_2 flexible surfaces have been evaluated by water contact measurements. The water contact angle of ZnO/SiO_2 before the surface modification by air plasma was 102.0° ± 1.3° and decreased to 38.7 ± 2.7° after plasma treatment for 64 s (Table S2). Similarly, the water contact angle of TiO_2/SiO_2 before the surface modification by air plasma was 127° ± 1.4° and decreased to 12.0 ± 0.9° after plasma treatment for 64 s. The considerable decrease of the water contact angle can be explained by the increase of the polar part of the surface energy, which is characteristic of surfaces treated in oxidative plasma (Homola et al., 2013).

The surface properties of ZnO/SiO_2 and TiO_2/SiO_2 flexible surfaces have been further evaluated by X-ray photoelectron spectroscopy (XPS) to determine the changes in surface chemistry before and after the modification in the plasma. The hydrophobic (WCA = 102.0° ± 1.3°, plasma untreated) ZnO/SiO_2 showed 7.9 at.% of zinc, 22.7 at.% of silicon, 44.8 at.% of oxygen and 22.6 at.% of carbon. On the other hand, the hydrophilic (WCA = 38.7° ± 2.7°, plasma untreated) ZnO/SiO_2 showed 22.6 at.% of zinc, 10.5 at.% of silicon, 48.7 at.% of oxygen and 10.7 at.% of carbon. Both samples showed a small amount of nitrogen, 2 at.% for untreated hydrophobic surface and 3.6 at.% for plasma-treated hydrophilic surface. The trend in the element concentration after the plasma treatment is, however, different than that observed in our previous work, for TiO_2/SiO_2 (Homola et al., 2016; Levchuk et al., 2019). The atomic concentration of the titanium and silicon in TiO_2/SiO_2 films remained roughly constant after the plasma treatment and plasma affected mainly the organo-silica surface. However, the concentration of zinc and silicon in ZnO/SiO_2 films was significantly affected by the plasma treatment, which resulted in higher atomic concentration of zinc and lower

atomic concentration of silicon, after the plasma treatment. The atomic concentration of elements in ZnO/SiO_2 and TiO_2/SiO_2 coatings is summarized in Table S3. Both plasma-treated coatings showed significant decrease in atomic concentration of carbon, which is the result of plasma oxidation and removal of organic moieties from the organo-silica binder and its transformation towards inorganic SiO_2.

The different behavior of plasma-treated ZnO is also apparent from SEM morphological images (Figure 4). Whereas the TiO_2/SiO_2 surfaces showed no difference between untreated and plasma-treated samples (Levchuk et al., 2019), the plasma treatment of ZnO/SiO_2 yields intensive changes in the morphology. The untreated ZnO/SiO_2 shows mesoporous surface with grains of 50 – 200 nm in diameter. On the other hand, the plasma-treated ZnO/SiO_2 shows considerable damage to the mesoporous structure – indicating presumably the damage in the silica film – as the atomic concentration of silicon decreased from 22.7 at. % to 10.5 at. % after plasma treatment for 64 s. The damage in the silica film that covers the ZnO surface can be explained by photo-corrosion of the ZnO surface triggered by exposure of ZnO to UV generated by plasma. The photo-corrosion is the major drawback of ZnO; however it can be inhibited by fullerenes or reduced graphene oxide (Lee et al., 2016)

Figure 4. SEM images of ZnO/SiO_2 thin films before (A, C) and after plasma treatment (B, D).

The XRD provides further evidence on lattice parameters of ZnO/SiO_2 surfaces treated by plasma. Figure 5 compares XRD diffraction patterns of untreated and plasma-treated ZnO/SiO_2. The diffraction patterns consist of the various ZnO crystal structure reflections. The most intensive are located at 31.8°, 34.4° and 36.3° and can be ascribed to (100), (002) and (101) diffractions corresponding to ZnO phase with the hexagonal lattice in the P63mc(186) space group (PDF card no. 00-033-1451). When Sherrer equation is used to calculate the grain size, (100), (002) and (101) showed a grain size

of 91 nm, 125 nm and 84 nm, respectively. No effect of plasma treatment on crystalline structure of ZnO was noticed and therefore it can be concluded that plasma treatment generates predominantly corrosion of the ZnO surface that led to structural changes of the organosilica binder.

Figure 5. XRD diffraction patterns of untreated and plasma-treated ZnO/SiO_2 coatings before (hydrophobic) and after (hydrophilic) plasma treatment

For TiO_2/SiO_2 coatings peaks located at 25.3°, 37.8° and 48.8° were identified and assigned to (101), (004) and (200) diffractions of crystalline phase of anatase. Characteristic peak of rutile phase (27.5°) with crystalline orientation (110) was also detected. The grain sizes calculated using Sherrer equation were 26 nm, 25 nm, 26 nm and 56 nm for (101), (004), (200) and (110), respectively (Homola et al., 2016).

3.3.2 Photocatalytic inactivation

Photocatalytic inactivation of *C. gillenii* present in RAS water streams was conducted using TiO_2/SiO_2 and ZnO/SiO_2 thin films under UV-LEDs radiation (λ=262 nm). The incidence of UV-C light into the surface of the photocatalyst leads to the generation of reactive oxygen species (ROS) (Eq. 5-7), able to cause external and internal damage to bacteria (Byrne et al., 2018; Ganguly et al., 2018).

$$\text{Photocatalyst} + h\upsilon \rightarrow h^+_{VB} + e^-_{CB} \qquad \text{Eq. (5)}$$

$$e^-_{CB} + O_2^- \rightarrow {}^{\bullet}O_2^- / HO_2^{\bullet} \qquad \text{Eq. (6)}$$

$$h^+_{VB} + H_2O \rightarrow {}^{\bullet}OH + H^+ \qquad \text{Eq. (7)}$$

The TiO_2/SiO_2 and ZnO/SiO_2 coatings were used in photocatalytic tests after air plasma treatment during 64 s. Reference tests were performed in absence of photocatalyst (UV-C photolysis) and in absence of UV-C radiation. No evaporation of test water during the photocatalytic experiments was observed. Results of photocatalytic inactivation of *C.*

gillenii as a function of UV dose are presented in Figure 6. Both types of photocatalytic thin films accelerated *C. gillenii* inactivation as compared to UV-C photolysis. Kinetic rate constants were increased up to 1.44 ± 0.29 $cm^2 \cdot mJ^{-1}$ and 1.91 ± 0.44 $cm^2 \cdot mJ^{-1}$ when TiO_2/SiO_2 and ZnO/SiO_2 thin films were used, respectively (Fig. 6B). In comparison with UV-C, photocatalytic disinfection with ZnO/SiO_2 and TiO_2/SiO_2 lead to the improvement of *C. gillenii* inactivation rates up to 55.3% and 17.5%, respectively. The UV dose required for reaching the 5 LRV was estimated to be about 4.35 $mJ \cdot cm^{-2}$ and 6.43 $mJ \cdot cm^{-2}$ when ZnO/SiO_2 and TiO_2/SiO_2, respectively (Figure 6A). Thus, photocatalytic treatment of RAS stream water using ZnO/SiO_2 reach 5 LRV for *C. gillenii* faster in comparison with TiO_2/SiO_2 and UV-C only. Higher efficiency of ZnO/SiO_2 than that of TiO_2/SiO_2 can be possibly explained by factors mentioned below. Adhesion of bacteria to the surface of the material is an important factor affecting efficiency of photocatalytic water disinfection (Pablos et al., 2013; Tallósy et al., 2016). According to earlier studies (Tallósy et al., 2016) higher adhesion onto photocatalyst surface may lead to higher efficiency of disinfection. In this study, RAS stream water was stirred in presence of photocatalyst in dark during 15 min before switching on UV-LEDs and viability of *C. gillenii* was measured. Inactivation of *C. gillenii* after 15 min in contact with TiO_2/SiO_2 and ZnO/SiO_2 (in absence of UV-C) was estimated to be 0.32 LRV and 1.04 LRV, respectively. Similar results were observed during reference test conducted in absence of UV-C radiation and in presence of photocatalyst. Higher bacteria inactivation detected for ZnO/SiO_2 coatings can be possibly attributed to *(i)* higher adhesion of *C. gillenii* onto the surface of ZnO/SiO_2 as compared to TiO_2/SiO_2 and/or *(ii)* leaching of zinc species possessing antimicrobial activity from ZnO/SiO_2. On one hand, the morphology of thin films can play a significant role in adhesion behavior of microorganisms onto its surface as reported in excellent review (Elbourne et al.,

2017). In our case it is difficult to speculate the role of morphology of tested thin films on *C. gillenii* adhesion, other than to note that the mesoporous structure of ZnO/SiO_2 (Figure 4) was significantly damaged, whereas opposite was true for TiO_2/SiO_2. On the other hand, higher toxicity of ZnO in dark as compared to TiO_2 was reported in earlier studies for *Escherichia coli* (Leung et al., 2016) and *Vibrio fischeri* (Heinlaan et al., 2008) which was explained by relatively high solubility of Zn ions from ZnO.

Figure 6. A. Inactivation profiles obtained for photocatalytic processes. Dark period (UV-off) =15 min. Experimental points are fitted to Log-lineal + tail inactivation model (lines). **B.** Maximum kinetic rate constant of inactivation obtained for photocatalytic processes. k_{max} is expressed in terms of UV-Dose, $cm^2 \cdot mJ^{-1}$. Bacterial indicator: *Citrobacter gillenii.*

Decrease of *E. coli* inactivation rates was reported when TiO_2 nanoparticles (1.0 $g \cdot L^{-1}$) were used under UV-LEDs radiation (λ = 265 nm and 275 nm) in comparison with UV only, which was attributed to screening effect produced by TiO_2 (Nyangaresi et al., 2019). Similar results were reported when lower concentration of TiO_2 nanoparticles (0.25 $g \cdot L^{-1}$) was applied for photocatalytic *E. coli* inactivation under UV-C radiation and decrease of disinfection rate, in presence of TiO_2, was explained by screening effect (Benabbou et al., 2007). However, when immobilized TiO_2 thin films were used in seawater under UV-C (λ=254 nm), inactivation of *Alteromonas sp* and *Corynebacterium stationis* was enhanced in comparison with UV-C only (Rubio et al., 2013). Thus, 99.9% reduction was reached at UV doses 13.1 $mJ \cdot cm^{-2}$ (*Corynebacterium stationis*) and 25.9 $mJ \cdot cm^{-2}$ (*Alteromonas sp*), which was about 30–33 % lower than UV doses required for achieving same level of disinfection only under UV-C. Similar observations were reported with immobilized TiO_2 under UV-C radiation for treatment of ballast water (Zhang et al., 2014).

3.4 Preliminary operational cost estimation

In general, the equipment cost for UV-C -LEDs are about two-four times higher than that of conventional UV-C lamps (considering same flow rate) (Peterson, 2020). However, maintenance is one of the major costs of the mercury lamps (replacements) which is negligible when UV-LEDs are used. Therefore, the electrical consumption of UV-LEDs gives the highest contribution to the operational cost as the maintenance costs are negligible. It should be stressed that electrical consumption of pumps, peripheral electric devices and maintenance were not included in this estimation. This is due to the fact that all experiments were conducted in laboratory scale and needed parameters for UV-C -LEDs at pilot scale are not readily available.

Preliminary operational costs were estimated for photolytic, photochemical and photocatalytic disinfection using UV doses required for achievement of 5 LRV. The electrical consumption (EC) of UV-LEDs per volume was estimated using Eq. (8).

$$EC = \frac{I \cdot V \cdot h}{Vol} \ (Wh \cdot L^{-1} \text{ or } kWh \cdot m^{-3}) \qquad \text{Eq. (8)}$$

*Where I is electrical current (A), V is input voltage (V), h is exposition time (h) and Vol is illuminated volume (L).

The prices of H_2O_2, PDS and PMS were estimated to be 0.70 € per kg (Baresel et al., 2019), 0.74 €/kg and 2.2 €/kg (Wacławek et al., 2017), respectively. As RAS installation was located in Finland, the price of electricity for industry in Finland was considered to be 0.067 €/kWh (BMWi. Statista, 2017). Estimated operational cost of photolytic disinfection of RAS stream water using UV-C -LEDs was 0.17 €/m^3. Results of preliminary operational cost evaluation are shown in Table 4.

Table 4. Preliminary cost estimation of photolytic, photochemical and photocatalytic treatment methods for disinfection of RAS water. The UV dose was chosen for 5 LRV inactivation of *Citrobacter gillenii*.

Results of preliminary estimation revealed that cost of studied photochemical disinfection methods was equal or lower than that of photolytic treatment. As it can be seen, the electrical consumption is the main cost of the photochemical treatment (Table 4). Among tested photochemical methods, the lowest costs were estimated for UV/H_2O_2 process. Interestingly, with increase of H_2O_2 dose from 5 to 10 mg·L^{-1}, the cost of the treatment decreases due to significant reduction of required UV dose (5 LRV). Whereas the opposite was true in case of UV/PDS process, and keep similar for the UV/PMS system. Total cost for photocatalytic disinfection presented in Table 4 does not include cost of photocatalyst. This is due to the fact that durability of prepared photocatalytic coatings was not tested in the scope of this study. Hence, the time when photocatalyst should be replaced is not known. However, an attempt to estimate the cost of photocatalytic material was made. The costs of TiO_2 and ZnO ink preparation are shown in Figure 7.

Figure 7. Cost estimation for 1L of TiO_2 and ZnO ink

Taking into account geometrical surface area of photocatalyst to volume of treated water used in this study, 61.25 m^2 of photocatalyst surface would be needed for reactor able to treat 1 m^3 of water (taking into account the required disinfection dose and performance, 5 LRV). According to our estimations, the price of photocatalyst deposition (coating with thickness of about 250 nm) is 0.06 €/m^2 and plasma pretreatment of photocatalytic coatings is 0.06 €/m^2. Thus, the preparation of photocatalyst (price for preparation of ZnO/SiO_2 and TiO_2/SiO_2 are similar) for reactor design of 1 m^3 of water would cost 7.35 € (for 61.25 m^2). In our earlier study (Levchuk et al., 2019), the photocatalytic activity of TiO_2/SiO_2 coatings for solar disinfection of seawater decreased after 10 cycles (15 h of contact between seawater and coating), which was attributed to deposition of salts on the surface of material. If we consider that

photocatalyst should be replaced after each 15 h (the worst scenario), the amount of treated RAS stream water would be around 600 m^3 (considering average dose of photocatalytic disinfection) and the cost of photocatalyst would be 0.012 €/m^3. So, the total cost of the photocatalytic disinfection can be estimated about 0.10 €/m^3 for ZnO/SiO_2 and 0.13 €/m^3 for TiO_2/SiO_2 (the electrical consumption cost was lower when ZnO/SiO_2 was used as compared to TiO_2/SiO_2). However, one should keep in mind that seawater is more aggressive for photocatalytic materials than fresh water, which means that in case of studied RAS water the cost of photocatalyst can be lower than in our estimation. Obtained results suggest that photocatalytic disinfection can be promising as it is effective and economically viable (in accordance with preliminary cost estimation) treatment for RAS water. However, as it was already mentioned before the durability of photocatalytic thin films for RAS water disinfection should be studied in the future to estimate the costs of this process more precisely.

Based on preliminary cost evaluation it can be suggested that UV/H_2O_2 (10 mg·L^{-1} of H_2O_2) and photocatalytic disinfection (ZnO/SiO_2 and TiO_2/SiO_2) processes are those with the lowest treatment cost, among tested disinfection methods. Finally, it should be mentioned that these economic estimations are based on laboratory tests performed in this study, and present a comparative purpose between the different inactivation processes studied. These estimates are likely to vary if applied on an industrial scale, where the design of photolytic reactors becomes critical due to optimizing radiation distribution and related energy consumption.

4. Conclusions

In this study, different photolytic, photochemical and photocatalytic processes have been tested for disinfection of real RAS water stream. Inactivation profiles of naturally occurring bacteria have been defined and the inactivation efficacy of each process has been obtained. Firstly, the use of different wavelengths (λ = 262 and 268 nm) in the UV-C spectra shows similar inactivation results. Otherwise, with the combination of both wavelengths (λ = 262+268 nm), slightly higher inactivation rates were obtained for both *Aeromonas hydrophila* and *Citrobacter gillenii*. Regarding photochemical process, the different oxidants (H_2O_2, PDS and PMS) in combination with UV-LEDs (λ = 262 nm) enhanced the disinfection rates in the range 15-38%. Concentrations of at least 5 $mg \cdot L^{-1}$ of the oxidant are needed to improve single UV-C process. Finally, the photocatalytic processes notably improved the UV-C treatment by reaching an enhancement of the disinfection rate up to 55% with ZnO/SiO_2 photocatalyst.

A preliminary estimation of the costs for the different processes was projected. A total cost in the range 0.12-0.17 €/m^3 was estimated for the different photo-driven disinfection processes. Taking into account the lowest cost and inactivation efficacy, the UV/H_2O_2 can be considered as the most suitable disinfection method for RAS streams among photolytic, photochemical and photocatalytic treatments tested. Otherwise, other processes such as UV/PMS and photocatalytic processes, in which a promising disinfection effectiveness has been detected, should be studied in the future to estimate the global efficiency of these processes more precisely.

Acknowledgments:

Authors are grateful for the financial support for the research from FEDER Operational Programme “Junta de Andalucía-UCA” (TECNOHABs Project; Grant Reference “sol-201800108023-tra”; 2018-080/PV/I+D+I FEDER Junta Andalucía/PR). D.Sc. Juan Jose Rueda-Marquez is thankful for financial support from Academy of Finland within the project ″Combination of Advanced Oxidation Processes and Photobiotreatment for Sustainable Resource Recovery and Wastewater Reuse” (No. 322339, 2019-2022) and Tekniikan Edistämissäätiö (TES foundation, Finland, grant number 6120. This research was also supported by project 19-14770Y funded by Czech Science Foundation and by the project LM2018097 funded by Ministry of Education, Youth and Sports of Czech Republic. Special thanks to Pavel Souček (R&D Center for Low-Cost Plasma and Nanotechnology Surface Modifications (CEPLANT)), Tomáš Svoboda and Petr Dzik (Faculty of Chemistry, Brno University of Technology), for help with preparation and characterization of photocatalytic materials. J. Moreno-Andrés is grateful to Generalitat Valenciana (Spain) (APOSTD/2019/207) for his Post-Doctoral contract and the financial support from the European Social Fund (ESF).

5. References

Arvin, E., Pedersen, L.F., 2015. Hydrogen peroxide decomposition kinetics in aquaculture water. Aquac. Eng. 64, 1–7. https://doi.org/10.1016/j.aquaeng.2014.12.004

Attramadal, K.J.K., Øie, G., Størseth, T.R., Alver, M.O., Vadstein, O., Olsen, Y., 2012a. The effects of moderate ozonation or high intensity UV-irradiation on the microbial environment in RAS for marine larvae. Aquaculture 330–333, 121–129. https://doi.org/10.1016/J.AQUACULTURE.2011.11.042

Attramadal, K.J.K., Salvesen, I., Xue, R., Øie, G., Størseth, T.R., Vadstein, O., Olsen, Y., 2012b. Recirculation as a possible microbial control strategy in the production of marine larvae. Aquac. Eng. 46, 27–39. https://doi.org/10.1016/J.AQUAENG.2011.10.003

Badiola, M., Mendiola, D., Bostock, J., 2012. Recirculating Aquaculture Systems (RAS) analysis: Main issues on management and future challenges. Aquac. Eng. 51, 26–35. https://doi.org/10.1016/J.AQUAENG.2012.07.004

Baresel, C., Harding, M., Junestedt, C., 2019. Removal of pharmaceutical residues from municipal wastewater using UV/H2O2. IVL Swedish Environ. Res. Inst. 2019 Rep. B2354.

Beck, S.E., Ryu, H., Boczek, L.A., Cashdollar, J.L., Jeanis, K.M., Rosenblum, J.S., Lawal, O.R., Linden, K.G., 2017. Evaluating UV-C LED disinfection performance and investigating potential dual-wavelength synergy. Water Res. 109, 207–216. https://doi.org/10.1016/J.WATRES.2016.11.024

Benabbou, A.K., Derriche, Z., Felix, C., Lejeune, P., Guillard, C., 2007. Photocatalytic inactivation of Escherischia coli. Effect of concentration of TiO2 and microorganism, nature, and intensity of UV irradiation. Appl. Catal. B Environ. 76, 257–263. https://doi.org/10.1016/j.apcatb.2007.05.026

Bianco, A., Polo−López, M.I., Fernández−Ibáñez, P., Brigante, M., Mailhot, G., 2017. Disinfection of water inoculated with Enterococcus faecalis using solar/Fe(III)EDDS-H2O2or S2O82−process. Water Res. 118, 249–260. https://doi.org/10.1016/j.watres.2017.03.061

Blancheton, J.P., Attramadal, K.J.K., Michaud, L., d'Orbcastel, E.R., Vadstein, O., 2013. Insight into bacterial population in aquaculture systems and its implication. Aquac. Eng. 53, 30–39. https://doi.org/10.1016/j.aquaeng.2012.11.009

BMWi. Statista, 2017. Prices of electricity for industry in Finland from 1995 to 2017. (December 12, 2017). [WWW Document]. URL https://www.statista.com/statistics/595853/electricity-industry-price-finland/ (accessed 8.12.19).

Bolton, J.R., Linden, K.G., 2003. Standardization of Methods for Fluence (UV Dose) Determination in Bench-Scale UV Experiments. J. Environ. Eng. 129, 209–215. https://doi.org/10.1061/(ASCE)0733-9372(2003)129:3(209)

Bruni, L., Pastorelli, R., Viti, C., Gasco, L., Parisi, G., 2018. Characterisation of the intestinal microbial communities of rainbow trout (Oncorhynchus mykiss) fed with Hermetia illucens (black soldier fly) partially defatted larva meal as partial dietary protein source. Aquaculture 487, 56–63. https://doi.org/10.1016/J.AQUACULTURE.2018.01.006

Byrne, C., Subramanian, G., Pillai, S.C., 2018. Recent advances in photocatalysis for environmental applications. J. Environ. Chem. Eng. 6, 3531–3555. https://doi.org/10.1016/J.JECE.2017.07.080

Chen, J., Loeb, S., Kim, J.-H., 2017. LED revolution: fundamentals and prospects for UV disinfection applications. Environ. Sci. Water Res. Technol. 3, 188–202. https://doi.org/10.1039/C6EW00241B

Diana, J.S., Egna, H.S., Chopin, T., Peterson, M.S., Cao, L., Pomeroy, R., Verdegem, M., Slack, W.T., Bondad-Reantaso, M.G., Cabello, F., 2013. Responsible Aquaculture in 2050: Valuing Local Conditions and Human Innovations Will Be Key to Success. Bioscience 63, 255–262. https://doi.org/10.1525/bio.2013.63.4.5

Dominguez, S., Ribao, P., Rivero, M.J., Ortiz, I., 2015. Influence of radiation and TiO2 concentration on the hydroxyl radicals generation in a photocatalytic LED reactor. Application to dodecylbenzenesulfonate degradation. Appl. Catal. B Environ. 178, 165–169. https://doi.org/10.1016/J.APCATB.2014.09.072

Eisenberg, G.M., 1943. Colorimetric Determination of Hydrogen Peroxide. Ind. Eng. Chem. 15, 327–328. https://doi.org/10.1016/S0016-0032(22)90949-4

Elbourne, A., Crawford, R.J., Ivanova, E.P., 2017. Nano-structured antimicrobial surfaces: From nature to synthetic analogues. J. Colloid Interface Sci. https://doi.org/10.1016/j.jcis.2017.07.021

Ganguly, P., Byrne, C., Breen, A., Pillai, S.C., 2018. Antimicrobial activity of photocatalysts: Fundamentals, mechanisms, kinetics and recent advances. Appl. Catal. B Environ. 225, 51–75. https://doi.org/10.1016/J.APCATB.2017.11.018

Geeraerd, A.H., Valdramidis, V.P., Van Impe, J.F., 2005. GInaFiT, a freeware tool to assess non-log-linear microbial survivor curves. Int. J. Food Microbiol. 102, 95–105. https://doi.org/10.1016/j.ijfoodmicro.2004.11.038

Grégori, D., Benchenaa, I., Chaput, F., Thérias, S., Gardette, J.L., Léonard, D., Guillard, C., Parola, S., 2014. Mechanically stable and photocatalytically active TiO 2 /SiO 2 hybrid films on flexible organic substrates. J. Mater. Chem. A 2, 20096–20104. https://doi.org/10.1039/c4ta03826f

Heinlaan, M., Ivask, A., Blinova, I., Dubourguier, H.C., Kahru, A., 2008. Toxicity of nanosized and bulk ZnO, CuO and TiO2 to bacteria Vibrio fischeri and crustaceans Daphnia magna and Thamnocephalus platyurus. Chemosphere 71, 1308–1316. https://doi.org/10.1016/j.chemosphere.2007.11.047

Homola, T., Dzik, P., Veselý, M., Kelar, J., Černák, M., Weiter, M., 2016. Fast and low-temperature (70 °C) mineralization of inkjet printed mesoporous TiO2 photoanodes using ambient air plasma. ACS Appl. Mater. Interfaces 8, 33562–33571. https://doi.org/10.1021/acsami.6b09556

Homola, T., Matoušek, J., Kormunda, M., Wu, L.Y.L., Černák, M., 2013. Plasma treatment of glass surfaces using diffuse coplanar surface barrier discharge in ambient air. Plasma Chem. Plasma Process. 33, 881–894. https://doi.org/10.1007/s11090-013-9467-3

Homola, T., Shekargoftar, M., Dzik, P., Krumpolec, R., Ďurašová, Z., Veselý, M., Černák, M., 2017. Low-Temperature (70 °C) Ambient Air Plasma-Fabrication of Inkjet-Printed Mesoporous TiO2 Flexible Photoanodes. Flex. Print. Electron. 2, 035010. https://doi.org/10.1088/2058-8585/aa88e6

Hull, N.M., Linden, K.G., 2018. Synergy of MS2 disinfection by sequential exposure to tailored UV wavelengths. Water Res. 143, 292–300.

https://doi.org/10.1016/j.watres.2018.06.017

Jo, W.K., Tayade, R.J., 2014. New generation energy-efficient light source for photocatalysis: LEDs for environmental applications. Ind. Eng. Chem. Res. 53, 2073–2084. https://doi.org/10.1021/ie404176g

Kim, D.-K., Kim, S.-J., Kang, D.-H., 2017. Bactericidal effect of 266 to 279 nm wavelength UVC-LEDs for inactivation of Gram positive and Gram negative foodborne pathogenic bacteria and yeasts. Food Res. Int. 97, 280–287. https://doi.org/10.1016/J.FOODRES.2017.04.009

Klinger, D., Naylor, R., 2012. Searching for Solutions in Aquaculture: Charting a Sustainable Course. Annu. Rev. Environ. Resour. 37, 247–276. https://doi.org/10.1146/annurev-environ-021111-161531

Lado Ribeiro, A.R., Moreira, N.F.F., Li Puma, G., Silva, A.M.T., 2019. Impact of water matrix on the removal of micropollutants by advanced oxidation technologies. Chem. Eng. J. 363, 155–173. https://doi.org/10.1016/J.CEJ.2019.01.080

Lee, K.M., Lai, C.W., Ngai, K.S., Juan, J.C., 2016. Recent developments of zinc oxide based photocatalyst in water treatment technology: A review. Water Res. 88, 428–448. https://doi.org/10.1016/J.WATRES.2015.09.045

Leung, Y.H., Xu, X., Ma, A.P.Y., Liu, F., Ng, A.M.C., Shen, Z., Gethings, L.A., Guo, M.Y., Djurišic, A.B., Lee, P.K.H., Lee, H.K., Chan, W.K., Leung, F.C.C., 2016. Toxicity of ZnO and TiO2 to Escherichia coli cells. Sci. Rep. 6. https://doi.org/10.1038/srep35243

Levchuk, I., Kralova, M., Rueda-Márquez, J.J., Moreno-Andrés, J., Gutiérrez-Alfaro, S., Dzik, P., Parola, S., Sillanpää, M., Vahala, R., Manzano, M.A., 2018. Antimicrobial activity of printed composite TiO2/SiO2and TiO2/SiO2/Au thin films under UVA-LED and natural solar radiation. Appl. Catal. B Environ. 239, 609–618. https://doi.org/10.1016/j.apcatb.2018.08.051

Levchuk, I., Moreno-Andrés, J., Rueda-márquez, J.J., Dzik, P., Ángel, M., Sillanpää, M., Manzano, M.A., Vahala, R., 2019. Solar photocatalytic disinfection using ink-jet printed composite TiO2/SiO2 thin films on flexible substrate : Applicability to drinking and marine water. Sol. Energy 191, 518–529. https://doi.org/10.1016/j.solener.2019.09.038

Li, G.Q., Wang, W.L., Huo, Z.Y., Lu, Y., Hu, H.Y., 2017. Comparison of UV-LED and low pressure UV for water disinfection: Photoreactivation and dark repair of Escherichia coli. Water Res. 126, 134–143. https://doi.org/10.1016/j.watres.2017.09.030

Liang, C., Huang, C.F., Mohanty, N., Kurakalva, R.M., 2008. A rapid spectrophotometric determination of persulfate anion in ISCO. Chemosphere 73, 1540–1543. https://doi.org/10.1016/j.chemosphere.2008.08.043

Lund, I., Thorarinsdottir, R., Drengstig, A., Arvonen, K., 2013. Farming different species in RAS in Nordic countries: Current status and future perspectives. Aquac. Eng. 53, 2–13. https://doi.org/10.1016/J.AQUAENG.2012.11.008

Malayeri, A.H., Mohseni, M., Cairns, B., Bolton, J.R., 2016. Fluence (UV Dose) Required to Achieve Incremental Log Inactivation of Bacteria, Protozoa, Viruses and Algae. IUVA News 18, 4–6.

Martín-Sómer, M., Pablos, C., van Grieken, R., Marugán, J., 2017. Influence of light distribution on the performance of photocatalytic reactors: LED vs mercury lamps. Appl. Catal. B Environ. https://doi.org/10.1016/j.apcatb.2017.05.048

Martins, C.I.M., Eding, E.H., Verdegem, M.C.J., Heinsbroek, L.T.N., Schneider, O., Blancheton, J.P., d'Orbcastel, E.R., Verreth, J.A.J., 2010. New developments in recirculating aquaculture systems in Europe: A perspective on environmental sustainability. Aquac. Eng. 43, 83–93. https://doi.org/10.1016/J.AQUAENG.2010.09.002

Marugán, J., van Grieken, R., Sordo, C., Cruz, C., 2008. Kinetics of the photocatalytic disinfection of Escherichia coli suspensions. Appl. Catal. B Environ. 82, 27–36. https://doi.org/10.1016/j.apcatb.2008.01.002

Matafonova, G., Batoev, V., 2018. Recent advances in application of UV light-emitting diodes for degrading organic pollutants in water through advanced oxidation processes: A review. Water Res. 132, 177–189. https://doi.org/10.1016/J.WATRES.2017.12.079

Mattle, M.J., Kohn, T., 2012. Inactivation and Tailing during UV 254 Disinfection of Viruses: Contributions of Viral Aggregation, Light Shielding within Viral Aggregates, and Recombination. Environ. Sci. Technol. 120830135926005.

https://doi.org/10.1021/es302058v

Moreno-Andrés, J., Farinango, G., Romero-Martínez, L., Acevedo-Merino, A., Nebot, E., 2019. Application of persulfate salts for enhancing UV disinfection in marine waters. Water Res. 163, 114866. https://doi.org/10.1016/J.WATRES.2019.114866

Moreno-Andrés, J., Romero-Martínez, L., Acevedo-Merino, A., Nebot, E., 2017. UV-based technologies for marine water disinfection and the application to ballast water: Does salinity interfere with disinfection processes? Sci. Total Environ. 581–582, 144–152. https://doi.org/10.1016/j.scitotenv.2016.12.077

Nyangaresi, P.O., Qin, Y., Chen, G., Zhang, B., Lu, Y., Shen, L., 2019. Comparison of UV-LED photolytic and UV-LED/TiO2 photocatalytic disinfection for Escherichia coli in water. Catal. Today 335, 200–207. https://doi.org/10.1016/j.cattod.2018.11.015

Nyangaresi, P.O., Qin, Y., Chen, G., Zhang, B., Lu, Y., Shen, L., 2018. Effects of single and combined UV-LEDs on inactivation and subsequent reactivation of E. coli in water disinfection. Water Res. 147, 331–341. https://doi.org/10.1016/j.watres.2018.10.014

Oguma, K., Rattanakul, S., Bolton, J.R., 2016. Application of UV Light–Emitting Diodes to Adenovirus in Water. J. Environ. Eng. 142, 04015082. https://doi.org/10.1061/(ASCE)EE.1943-7870.0001061

Pablos, C., Van Grieken, R., Marugán, J., Chowdhury, I., Walker, S.L., 2013. Study of bacterial adhesion onto immobilized TiO2: Effect on the photocatalytic activity for disinfection applications. Catal. Today 209, 140–146. https://doi.org/10.1016/j.cattod.2012.12.010

Pedersen, L.-F., Pedersen, P.B., 2012. Hydrogen peroxide application to a commercial recirculating aquaculture system. Aquac. Eng. 46, 40–46. https://doi.org/10.1016/J.AQUAENG.2011.11.001

Pedersen, L.-F., Rojas-Tirado, P., Arvin, E., Pedersen, P.B., 2019. Assessment of microbial activity in water based on hydrogen peroxide decomposition rates. Aquac. Eng. 85, 9–14. https://doi.org/10.1016/J.AQUAENG.2019.01.001

Peterson, J., 2020. Toppling Existing Pricing Models for Low Flow Water Disinfection

Products with UVC LEDs [WWW Document]. Klaran Univ. URL https://www.klaran.com/toppling-existing-pricing-models-for-low-flow-water-disinfection-products-with-uvc-leds (accessed 5.2.20).

Piedrahita, R.H., 2003. Reducing the potential environmental impact of tank aquaculture effluents through intensification and recirculation. Aquaculture 226, 35–44. https://doi.org/10.1016/S0044-8486(03)00465-4

Pulkkinen, J.T., Kiuru, T., Aalto, S.L., Koskela, J., Vielma, J., 2018. Startup and effects of relative water renewal rate on water quality and growth of rainbow trout (Oncorhynchus mykiss) in a unique RAS research platform. Aquac. Eng. 82, 38–45. https://doi.org/10.1016/j.aquaeng.2018.06.003

Rantalankila, M., Koivistoinen, H., Sarvasidze, L., Sillanpää, M.E.T., 2016. Inactivation of Asterionellopsis glacialis in seawater using combinations of deep ultraviolet light emitting diodes. Sep. Purif. Technol. 169, 247–252. https://doi.org/10.1016/J.SEPPUR.2016.05.045

Rattanakul, S., Oguma, K., 2018. Inactivation kinetics and efficiencies of UV-LEDs against Pseudomonas aeruginosa, Legionella pneumophila, and surrogate microorganisms. Water Res. 130, 31–37. https://doi.org/10.1016/J.WATRES.2017.11.047

Ribeiro, R.S., Frontistis, Z., Mantzavinos, D., T Silva, A.M., Faria, J.L., Gomes, H.T., 2019. Screening of heterogeneous catalysts for the activated persulfate oxidation of sulfamethoxazole in aqueous matrices. Does the matrix affect the selection of catalyst? J. Chem. Technol. Biotechnol. jctb.6080. https://doi.org/10.1002/jctb.6080

Rizzo, L., Malato, S., Antakyali, D., Beretsou, V.G., Đolić, M.B., Gernjak, W., Heath, E., Ivancev-Tumbas, I., Karaolia, P., Lado Ribeiro, A.R., Mascolo, G., McArdell, C.S., Schaar, H., Silva, A.M.T., Fatta-Kassinos, D., 2019. Consolidated vs new advanced treatment methods for the removal of contaminants of emerging concern from urban wastewater. Sci. Total Environ. 655, 986–1008. https://doi.org/10.1016/J.SCITOTENV.2018.11.265

Rodríguez-Chueca, J., García-Cañibano, C., Lepistö, R.J., Encinas, A., Pellinen, J., Marugán, J., 2019. Intensification of UV-C tertiary treatment: Disinfection and

removal of micropollutants by sulfate radical based Advanced Oxidation Processes. J. Hazard. Mater. 372, 94–102. https://doi.org/10.1016/j.jhazmat.2018.04.044

Rodríguez-Chueca, J., Silva, T., Fernandes, J.R., Lucas, M.S., Puma, G.L., Peres, J.A., Sampaio, A., 2017. Inactivation of pathogenic microorganisms in freshwater using HSO5−/UV-A LED and HSO5−/Mn+/UV-A LED oxidation processes. Water Res. 123, 113–123. https://doi.org/10.1016/j.watres.2017.06.021

Romero-Martínez, L., Moreno-Andrés, J., Acevedo-Merino, A., Nebot, E., 2014. Improvement of ballast water disinfection using a photocatalytic (UV-C+TiO2) flow-through reactor for saltwater treatment. J. Chem. Technol. Biotechnol. 89, 1203–1210. https://doi.org/10.1002/jctb.4385

Rubio, D., Casanueva, J.F., Nebot, E., 2013. Improving UV seawater disinfection with immobilized TiO2: Study of the viability of photocatalysis (UV254/TiO2) as seawater disinfection technology. J. Photochem. Photobiol. A Chem. 271, 16–23. https://doi.org/10.1016/j.jphotochem.2013.08.002

Rurangwa, E., Verdegem, M.C.J., 2015. Microorganisms in recirculating aquaculture systems and their management. Rev. Aquac. 7, 117–130. https://doi.org/10.1111/raq.12057

Salvesen, I., Skjermo, J., Vadstein, O., 1999. Growth of turbot (Scophthalmus maximus L.) during first feeding in relation to the proportion of r/K-strategists in the bacterial community of the rearing water. Aquaculture 175, 337–350. https://doi.org/10.1016/S0044-8486(99)00110-6

Serna-Galvis, E.A., Salazar-Ospina, L., Jiménez, J.N., Pino, N.J., Torres-Palma, R.A., 2020. Elimination of carbapenem resistant Klebsiella pneumoniae in water by UV-C, UV-C/persulfate and UV-C/H2O2. Evaluation of response to antibiotic, residual effect of the processes and removal of resistance gene. J. Environ. Chem. Eng. 8, 102196. https://doi.org/10.1016/j.jece.2018.02.004

Song, K., Mohseni, M., Taghipour, F., 2016. Application of ultraviolet light-emitting diodes (UV-LEDs) for water disinfection: A review. Water Res. 94, 341–349. https://doi.org/10.1016/j.watres.2016.03.003

Song, K., Taghipour, F., Mohseni, M., 2019. Microorganisms inactivation by

wavelength combinations of ultraviolet light-emitting diodes (UV-LEDs). Sci. Total Environ. 665, 1103–1110. https://doi.org/10.1016/J.SCITOTENV.2019.02.041

Summerfelt, S.T., 2003. Ozonation and UV irradiation—an introduction and examples of current applications. Aquac. Eng. 28, 21–36. https://doi.org/10.1016/S0144-8609(02)00069-9

Sun, P., Tyree, C., Huang, C.H., 2016. Inactivation of Escherichia coli, Bacteriophage MS2, and Bacillus Spores under UV/H2O2and UV/Peroxydisulfate Advanced Disinfection Conditions. Environ. Sci. Technol. 50, 4448–4458. https://doi.org/10.1021/acs.est.5b06097

Takeda, K., Fujisawa, K., Nojima, H., Kato, R., Ueki, R., Sakugawa, H., 2017. Hydroxyl radical generation with a high power ultraviolet light emitting diode (UV-LED) and application for determination of hydroxyl radical reaction rate constants. J. Photochem. Photobiol. A Chem. https://doi.org/10.1016/j.jphotochem.2017.02.020

Tallósy, S.P., Janovák, L., Nagy, E., Deák, Á., Juhász, Á., Csapó, E., Buzás, N., Dékány, I., 2016. Adhesion and inactivation of Gram-negative and Gram-positive bacteria on photoreactive TiO2/polymer and Ag-TiO2/polymer nanohybrid films. Appl. Surf. Sci. 371, 139–150. https://doi.org/10.1016/j.apsusc.2016.02.202

Umar, M., Roddick, F., Fan, L., 2019. Moving from the traditional paradigm of pathogen inactivation to controlling antibiotic resistance in water - Role of ultraviolet irradiation. Sci. Total Environ. 662, 923–939. https://doi.org/10.1016/J.SCITOTENV.2019.01.289

Vadstein, O., Attramadal, K.J.K., Bakke, I., Olsen, Y., 2018. K-Selection as Microbial Community Management Strategy: A Method for Improved Viability of Larvae in Aquaculture. Front. Microbiol. 9, 2730. https://doi.org/10.3389/fmicb.2018.02730

Vilhunen, S., Puton, J., Virkutyte, J., Sillanpää, M., 2011. Efficiency of hydroxyl radical formation and phenol decomposition using UV light emitting diodes and H2O2. Environ. Technol. 32, 865–872. https://doi.org/10.1080/09593330.2010.516770

Wacławek, S., Grübel, K., Černík, M., 2015. Simple spectrophotometric determination of monopersulfate. Spectrochim. Acta - Part A Mol. Biomol. Spectrosc. 149, 928–

933. https://doi.org/10.1016/j.saa.2015.05.029

Wacławek, S., Lutze, H. V., Grübel, K., Padil, V.V.T., Černík, M., Dionysiou, D.D., 2017. Chemistry of persulfates in water and wastewater treatment: A review. Chem. Eng. J. 330, 44–62. https://doi.org/10.1016/j.cej.2017.07.132

Wen, G., Zhao, D., Xu, X., Chen, Z., Huang, T., Ma, J., 2019. Inactivation of fungi from four typical genera in groundwater using PMS/Cl−system: Efficacy, kinetics and mechanisms. Chem. Eng. J. 357, 567–578. https://doi.org/10.1016/j.cej.2018.09.195

Xiao, R., Liu, K., Bai, L., Minakata, D., Seo, Y., Kaya Göktaş, R., Dionysiou, D.D., Tang, C.-J., Wei, Z., Spinney, R., 2019. Inactivation of pathogenic microorganisms by sulfate radical: Present and future. Chem. Eng. J. 371, 222–232. https://doi.org/10.1016/J.CEJ.2019.03.296

Zhang, N., Hu, K., Shan, B., 2014. Ballast water treatment using UV/TiO2 advanced oxidation processes: An approach to invasive species prevention. Chem. Eng. J. 243, 7–13. https://doi.org/10.1016/j.cej.2013.12.082

LIST OF FIGURES:

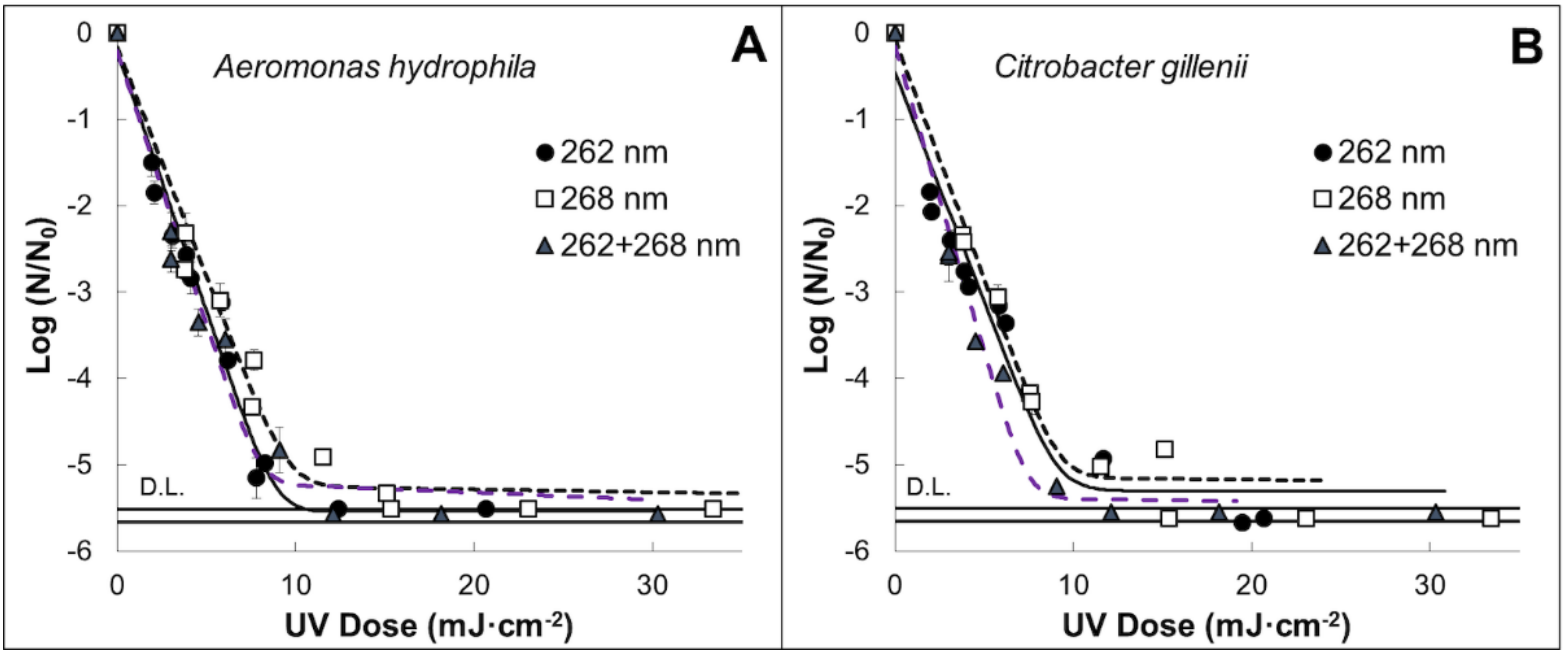

Figure 1. Inactivation profiles obtained for photolytic processes and for two different naturally occurring bacteria in RAS streams. **A.** *A. hydrophila* and **B.** *C. gillenii*. Experimental points are fitted to Log-lineal + tail inactivation model (lines). The coefficient of variation of each experimental point does not exceed 15%.

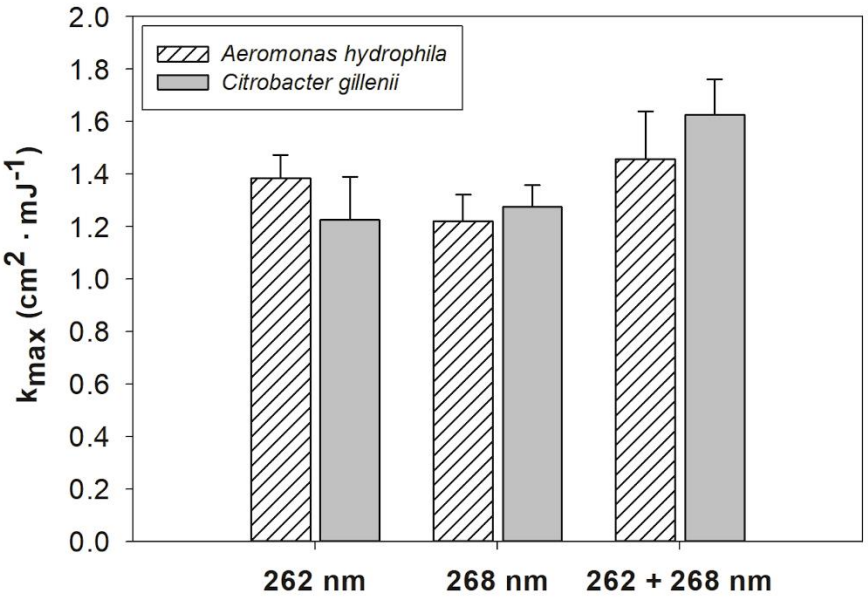

Figure 2. Maximum kinetic rate constant of inactivation obtained for photolytic treatment at different wavelengths. k_{max} is expressed in terms of UV-Dose, $cm^2 \cdot mJ^{-1}$. Error bars represent Standard Error.

TABLES:

Table 1. Characterization of RAS stream, as the water matrix used in the experimentation.

Parameter	**Value ± S.D.**	
pH	7.01 ± 0.10	
Conductivity ($mS \cdot cm^{-1}$)	0.62 ± 0.07	
UV-Transmittance (%)	262 nm	268 nm
	37.05 ± 6.01	43.65 ± 1.05
Total Organic Carbon (TOC) ($mg\ C \cdot L^{-1}$)	14.66 ± 1.88	

Table 2. Bacterial identification in water samples from the RAS.

Strain code (GenBank accession no.)	**Identification**	
	BLAST	**Similarity**
NBRC 13784 (NR113635.1)	*Aeromonas salmocida*	95.42%
ATCC 7966 (NR074841.1)	*Aeromonas hydrophila*	91.90%
DSM 8802T (NR115063.1)	*Bacillus halotolerans*	84.90%
GS2 (CP013913.1)	*Serratia fonticola*	93.34%
SH1(KY784653.1)	*Citrobacter gillenii*	95.99%
MF429365.1	*Lactococcus lactis*	96.41%

Table 3. Kinetic parameters obtained after the application of different photochemical systems at different concentrations of H_2O_2, PDS and PMS. It has been obtained through modelling of experimental points through the Log-linear + tail model (R^2 > 0.94; RMSE: 0.33-0.51). Bacterial indicator: *Citrobacter gillenii.*

[H_2O_2 / PDS / PMS] ($mg \cdot L^{-1}$)	k_{max} ± S.E.	5 LRV
	$cm^2 \cdot mJ^{-1}$	$mJ \cdot cm^{-2}$
UV (λ_{262})		
0	1.23 ± 0.16	9.32
UV/H_2O_2		
1	1.26 ± 0.10	8.69
5	1.45 ± 0.16	7.69
10	1.78 ± 0.33	5.99
UV/PDS		
1	1.03 ± 0.14	9.72
5	1.48 ± 0.23	7.61
10	1.41 ± 0.18	7.94
UV/PMS		
1	1.30 ± 0.14	8.49
5	1.50 ± 0.14	7.34
10	1.53 ± 0.19	7.03

Table 4. Preliminary cost estimation of photolytic, photochemical and photocatalytic treatment methods for disinfection of RAS water. The UV dose was chosen for 5 LRV inactivation of *Citrobacter gillenii*.

Treatment method		UV dose for reach 5 LRV ($mJ\ cm^{-2}$)	Time (h)	Electrical consumption ($kWh\ m^{-3}$)	Reagent cost (€ cent m^{-3})	Total cost (€ m^{-3})
UV-LED (λ_{262})						
UV		9.32	0.041	2.5	--	0.17
Photochemical						
UV/H_2O_2	5 $mg \cdot L^{-1}$	7.69	0.035	2.1	0.35	0.14
	10 $mg \cdot L^{-1}$	5.99	0.028	1.7	0.7	0.12
UV/PDS	5 $mg \cdot L^{-1}$	7.61	0.035	2.1	0.35	0.15
	10 $mg \cdot L^{-1}$	7.94	0.040	2.4	0.7	0.17
UV/PMS	5 $mg \cdot L^{-1}$	7.34	0.033	2.0	1.1	0.15
	10 $mg \cdot L^{-1}$	7.03	0.035	2.1	2.2	0.16
Photocatalytic						
UV/ZnO/SiO_2		4.35	0.020	1.2	--	0.08
UV/TiO_2/SiO_2		6.43	0.029	1.7	--	0.12

SUPPLEMENTARY MATERIAL:

Table S1. Water quality in the systems during the sampling. NH_4^+, NO_2^- , and NO_3^- (mg $N \cdot L^{-1}$) ; Alk.: Alkalinity (mg $CaCO_3 \cdot L^{-1}$).

TANK nº 5				
NH_4^+-N	**NO_2^- -N**	**NO_3^- -N**	**Alk.**	**pH**
0.65	0.109	47.6	23.8	7.04
0.77	0.117	57.4	23.5	7.01
0.7	0.093	60.8	21.4	6.92
0.56	0.053	46.4	25.8	7.12
TANK nº 8				
0.49	0.072	49.6	19.3	7
0.51	0.087	57.2	19.2	6.99
0.63	0.082	56.2	18.7	7.11
0.49	0.067	51.4	20.2	7.05

Table S2. Water contact angle for photocatalytic thin films measured before (0 s) and after plasma (64 s) treatment.

Material	**Treatment time (s)**	**WCA (°)**	**WCA error (°)**
ZnO/SiO_2	0	102	1.3
	64	38.7	2.7
TiO_2/SiO_2	0	127	1.4
	64	12	0.9

Table S3. Atomic concentration of elements measured by means of XPS in ZnO/SiO_2 and TiO_2/SiO_2 thin films

Material	**Treatment time**	**Zn2p**	**Si2p**	**O1s**	**C1s**	**N1s**
ZnO/SiO_2	0	7.87	22.66	44.84	22.62	2.02
	64	26.62	10.51	48.65	10.69	3.55
Material	**Treatment time**	**Ti2p**	**Si2p**	**O1s**	**C1s**	**Na1s**
TiO_2/SiO_2	0	9.28	16.48	50.34	21.63	2.27
	64	9.46	16.38	64.10	5.43	4.63